COLLOQUIA: LaThuile10

Studies of cosmic ray electrons with the Fermi-LAT

L. LATRONICO on behalf of the FERMI-LAT COLLABORATION

INFN, Sezione di Pisa - L.go B. Pontecorvo 3, 56127 Pisa, Italy

Summary. — The Fermi Large Area Telescope measures the cosmic-ray electron spectrum from 7 GeV up to 1 TeV, covering a broad range of approximately 2.5 decades with unprecedented accuracy. This result is based on an analysis of about 8 million electron candidates detected in the first 12 months of operations of the satellite. It extends our previously published measurement down to 7 GeV, and confirms a spectrum harder than expected and with no prominent spectral features. In this paper we describe key points of the analysis and of its validations, as well as a cross-check measurement of the spectrum via a subset of events selected for the best energy resolution. Possible interpretations of the result and prospects for future Fermi measurements are briefly discussed at the end.

PACS 95.85.Ry – Neutrino, muon, pion, and other elementary particles; cosmic rays.
PACS 96.50.sb – Composition, energy spectra and interactions.
PACS 95.35.+d – Dark Matter (stellar, interstellar, galactic, and cosmological).

1. – Introduction

The Fermi observatory was launched on June 11, 2008 into a circular orbit at 565 km altitude and 25.6° inclination. Since then, observations with the Large Area Telescope (LAT [1]), a pair conversion telescope that is the main instrument onboard, have opened a new and important window on a wide variety of phenomena. These include the discovery of a new population of pulsars pulsing only in gamma-rays, which provides new insight into some of the extreme accelerators in our Galaxy [2]; the detection of photons up to 10s of GeV from gamma-ray bursts, which transforms our understanding of the astrophysics of these extreme explosions [3]; a determination of the diffuse gamma-ray emission with unprecedented accuracy [4] providing new constraints on dark matter models [5]; the discovery of around a thousand new gamma-ray sources [6]. Continuous monitoring of the high-energy gamma-ray sky has uncovered numerous outbursts from active Galaxies and the discovery of as-yet-unidentified transients from the direction of our Galaxy([1]). Some

---

([1]) `https://www-glast.stanford.edu/cgi-bin/pub_rapid`

11

high-sensitivity gamma-ray observations that are most relevant for cosmic-ray physics are discussed in an accompanying paper (Knödlseder, these proceedings). Beyond these, the LAT Collaboration also provided the first high-precision, systematics-limited measurement of the cosmic-ray electron (CRE) spectrum from 20 GeV to 1 TeV, which indicates an excess in the high energy CRE spectrum with respect to most pre-Fermi experiments and conventional cosmic-ray diffusion and propagation models [7].

2. – The Cosmic-Ray Electron spectrum

CREs with energy greater than ~ 100 GeV lose their energy rapidly ($-\mathrm{d}E/\mathrm{d}t \propto E^2$) by synchrotron radiation on Galactic magnetic fields and by inverse Compton scattering (IC) on the interstellar radiation field. The typical distance over which a 1 TeV CRE loses half its total energy is estimated to be 300–400 pc (see, *e.g.*, [8]) when it propagates within about one kpc of the Sun. This makes them a unique tool for probing nearby Galactic space.

Recent results from the ATIC [9], PPB-BETS [10], H.E.S.S. [11,12], PAMELA [13], and Fermi LAT [7] have shed new light on the origin of CREs. The ATIC and PPB-BETS teams reported evidence for an excess of electrons in the range 300–700 GeV compared to the background expected from a conventional homogeneous distribution of cosmic-ray (CR) sources. The H.E.S.S. team reported a spectrum that steepens above ~ 900 GeV, a result which is consistent with an absence of sources of electrons above ~ 1 TeV within 300–400 pc. The PAMELA Collaboration reports that the ratio of the positron flux to the total flux of electrons and positrons increases with energy, a result which has significant implications. The Fermi result either requires a reconsideration of the source spectrum and/or the propagation model or indicates the presence of a nearby source. However, the excess of events reported by ATIC and PPB-BETS was not detected by the LAT.

2˙1. *Event selection and validations*. – The LAT photon analysis is currently optimized for the 100 MeV–300 GeV range, but we demonstrated that a direct measurement of high energy electrons can be performed with great accuracy from a few GeV and up to 1 TeV by using a dedicated event analysis.

The event selection process must balance removal of the overwhelming background events of hadronic origin and retaining signal events, while limiting systematic uncertainties. We first reject those events that are badly reconstructed or are otherwise unusable. The next step is to select electron candidates based on the detailed event patterns in the calorimeter, the tracker and the ACD subsystems.

Generally, the shapes of hadronic showers differ significantly from electromagnetic (EM) showers. EM cascades are tightly confined, while hadronic cascades that leave comparable energy in the calorimeter tend to deposit energy over a much wider lateral region affecting all three detector subsystems. The nuclear fragments tend to leave energy far from the main trajectory of the particle. Thus hadron showers have larger transverse sizes in the calorimeter, larger numbers of stray tracks in the tracker and larger energy deposits in more ACD tiles. Therefore, the most powerful separators are the comparative lateral distributions and the event selection relies on the capabilities of the tracker, calorimeter and anticoincidence subsystems of the LAT, alone and in combination to discriminate between EM and hadronic event topologies.

Since the phenomenology of the EM cascades and hadron interactions varies dramatically over the energy range of interest, we developed two independent event selections,

one tuned for energies between 20 and 1000 GeV and the other for energies between 0.1 and 100 GeV, which we shall refer to as HE and LE. The HE analysis takes advantage of the fact that the on-board filtering (event selections designed to fit the data volume into the available telemetry bandwidth with a minimal impact on the photon yield) is disengaged for events depositing more than 20 GeV in the calorimeter. The source of data for the LE selection is an unbiased sample of all trigger types, prescaled (on-board) by a factor 250, which is continuously down-linked for diagnostic purposes. The region of overlap in energy, between 20 and 80 GeV, allows us to cross-check the two independent analyses. Above about 80 GeV the number of events in the prescaled sample becomes too low to be useful.

Finally, and similarly to what we do for selecting photons [1], a Classification Tree (CT) analysis(^{2}) provides the remaining necessary hadron rejection power. Starting from the same quantities (variables) defined in the photon event reconstruction, we identify those that are most sensitive to the differences between EM and hadronic event topologies and build CTs that for each event, based on large simulated training datasets, predict the probability that the event is an electron. Examples of powerful discriminants are the multiplicity of tracks and the extra hits outside of reconstructed tracks in the tracker and several variables mapping the 3-dimensional shower development in the calorimeter. The cut that we have adopted on the resulting CT-predicted electron probability is energy dependent. For HE analysis, a higher probability is required as energy increases. These cuts give us a set of candidate electron events.

As simulations are the starting point for the event selection, we systematically compare them with the flight data. Any variables for which the data-MC agreement was not satisfactory were not used in any part of the selection. Figure 1 shows an example of the data-MC comparison for the CT electron probabilities. The input energy spectra for all the particles are those included in the model of energetic particles in the Fermi orbit [1], with the exception of the electrons that follow instead a power law spectrum that fits our previous publication [7].

2`2. *Energy resolution validations*. – Since showers above 20 GeV are not fully contained by the LAT calorimeter, the energy reconstruction is a critical step of this analysis. In order to cross check the impact of the energy resolution on the measured spectrum, we performed a dedicated analysis in which we selected events with the longest path lengths (at least 12 X_0) in the calorimeter. We further selected events that do not cross any of the boundary gaps between calorimeter tower modules and that have sufficient track length (at least 1 X_0) in the tracker for a good direction reconstruction. For the event sample defined by these three requirements the average amount of material traversed is $\sim 16\ X_0$, ensuring that the shower maximum is well contained in the calorimeter up to at least 1 TeV (the average depth of the shower maximum for electrons at this energy is 10.9 X_0). Correspondingly the instrument acceptance decreases to $\sim 5\%$ of that achieved in the standard analysis described in the previous sections. As illustrated in fig. 2, the energy resolution for events passing this restrictive selection is significantly better than that for the full analysis. The energy dispersion distributions are much narrower and symmetric, with no prominent low energy tails. The energy resolution (half width of the 68% containment window) is around 3% at 100 GeV and increases to approximately 5% at 1 TeV.

(^{2}) The reader can refer to [14] for a comprehensive review of the use of data mining and machine learning techniques in astrophysics.
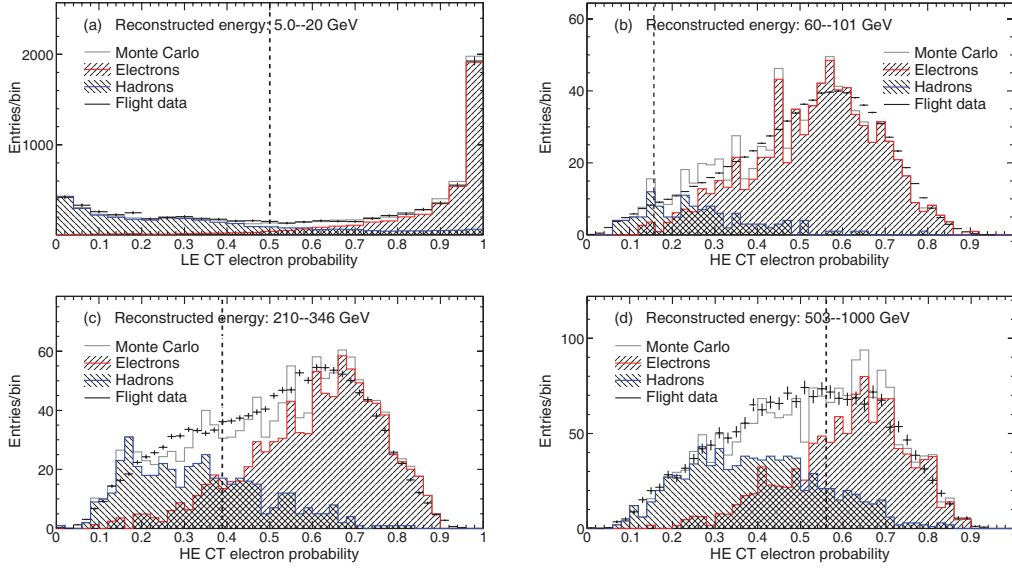
Fig. 1. – Distribution of CT predicted probability (a) for LE analysis and (b), (c) and (d) for HE analysis in different energy intervals. Monte Carlo generated distributions are compared with flight distributions. The cut value is a continuous function of energy and is represented by the vertical dashed line in each panel. The distributions are shown after the cuts on all other variables have been applied.

Figure 3 shows the consistency, within the systematic errors, between the spectrum obtained with the standard analysis and that obtained with the long-path selection. This confirms that the energy resolution quoted for the standard selection is indeed sufficient for the measurement and does not have any significant effect on the spectrum.
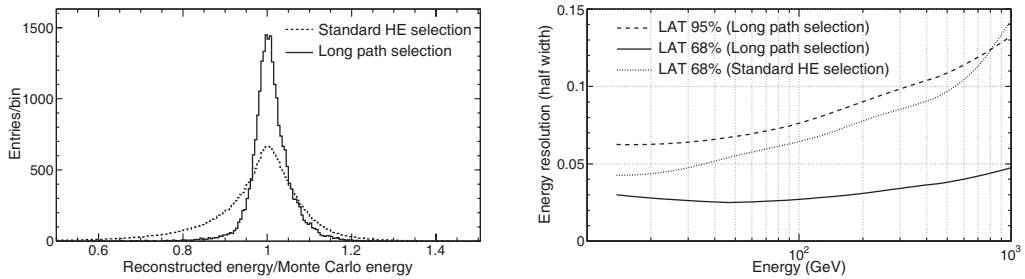

Fig. 2. – Left: energy dispersion distribution in the energy range 242–458 GeV for the long path selection (solid line) and the standard HE analysis (dashed line). Right: energy resolution for the long path selection analysis. The half width of the 68% containment window for the HE analysis, which is comparable with that of the 95% window for the more restrictive analysis, is overlaid for reference.
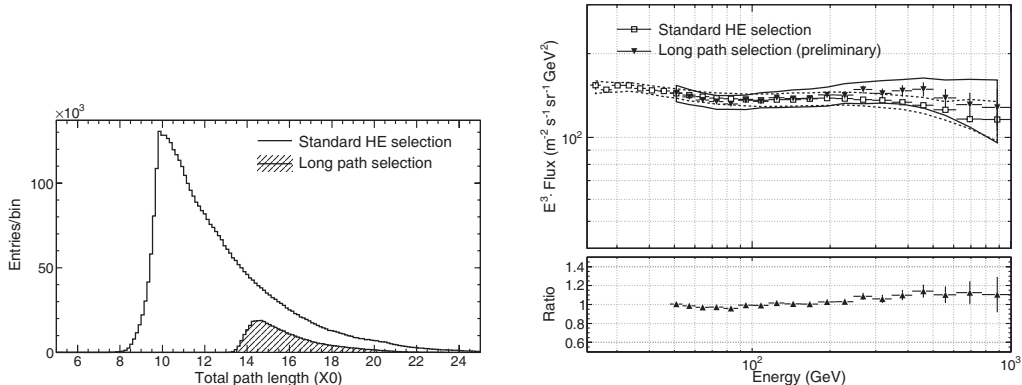
Fig. 3. – Left: distribution of the amount of material traversed by the candidate electrons passing the long path selection, compared with that for the entire data sample used in the standard analysis (the sharp edge at $\sim 10 \, X_0$ in the latter reflects the total thickness of the instrument on-axis). Note the difference in the number of events. Right: comparison of the spectra obtained with the long path selection and the standard HE selection. The continuous lines represent the systematic uncertainties. The bottom panel shows the ratio of the two spectra.

2˙3. *Low energy extension of the measurement.* – In order to extend the measurement to energies below $\sim 20 \, \mathrm{GeV}$, we need to consider the shielding effect of the geomagnetic field as characterized by the cutoff rigidity. The lowest allowed primary-electron energy is strongly dependent on geomagnetic position and decreases with increasing geomagnetic latitude. For the orbit of Fermi, the cutoff ranges between about 6 and $15 \, \mathrm{GeV}$.

As recognized in [15], the McIlwain L$(^3)$ parameter is particularly convenient for characterizing cutoff rigidities and has been used for selecting data in the LE analysis.

Each McIlwain L interval has an associated cutoff energy E_c that we determine by parameterizing the shape of the CRE spectrum as

$$(1) \qquad \frac{\mathrm{d}N}{\mathrm{d}E} = c_\mathrm{s} E^{-\Gamma_\mathrm{s}} + \frac{c_\mathrm{p} E^{-\Gamma_\mathrm{p}}}{1 + (E/E_c)^{-6}} \, ,$$

where c_s and c_p are the normalization constants for the secondary (albedo) and primary components of the spectrum while Γ_s and Γ_p are their spectral indexes.

Due to the complexity of the particle orbits in the Earth's magnetosphere, the transition to cutoff is smoothed out. Therefore, we increase E_c by 15% to arrive at an effective minimum energy of the primary electron flux not affected by the Earth's magnetic field. We split the LE data sample into 10 intervals of McIlwain L parameter. For each energy bin we use the interval of McIlwain L parameter whose effective minimum energy is lower than the energy in question. This procedure is illustrated in full details in [16] and in fig. 4, where the electron spectrum is shown across the full energy range accessible to this analysis and together with the McIlwain L intervals from which the flux was measured

---

$(^3)$ The McIlwain L parameter is a geomagnetic coordinate defined as the distance in Earth radii from the center of the Earth's titled, off-center, equivalent dipole to the equatorial crossing of a field line.
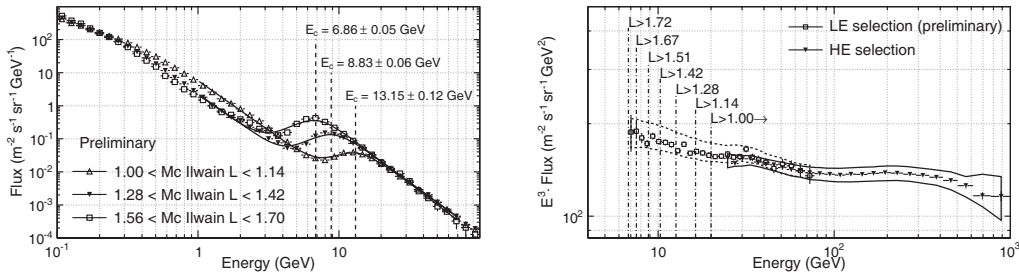
Fig. 4. – Left: the measured electron flux in three McIlwain L bins. For each bin the fit of the flux with eq. (1) and the resulting estimated cutoff rigidity, E_c, is shown. As described in the text, E_c decreases for larger values of McIlwain L. Right: cosmic-ray electron spectra as measured by Fermi LAT for one year of observations for LE events (squares) and HE events (triangles). The continuous lines represent the systematic uncertainties. The two spectra agree within systematic errors in the overlap region between 20 GeV and 80 GeV.

for the LE analysis. The same figure also shows a very nice overlap of the LE and HE independent analysis up to ~ 100 GeV, confirming the robustness of the result.

2'4. *Results and discussion.* – After electron candidates are selected, we derive event count rates dividing them by the observatory livetime. Similarly, we derive the count rate of residual hadronic events in the sample using a Monte Carlo simulation of the on-orbit background, and finally subtract this from the total count rate to get the CRE only count rate. Ultimately, we compute the CRE flux by scaling count rates in each predetermined energy bin with the corresponding effective geometric factor, that represents the instrument acceptance as determined from Monte Carlo simulations of pure electrons (see [17] for full details).

The resulting spectrum from all the data collected in nominal sky survey mode from 4 August 2008 to 4 August 2009 is shown in fig. 5.

The CRE spectrum reported here is essentially the same as that published in [7] for the energy above 20 GeV, but with twice the data volume. Within the systematic errors (shown by the grey band in fig. 5) the entire spectrum from 7 GeV to 1 TeV can be fitted by a power law with spectral index in the interval 3.03–3.13 (best fit $\propto E^{-3.08\pm0.05}$), similar to that given in [7]. The spectrum is significantly harder (flatter) than that reported by previous experiments. Below ~ 50 GeV the electron spectrum is consistent with previous experiments and does not indicate any flattening at low energies. The cross-check analysis using events with long paths in the instrument confirms the absence of any evident feature in the $e^+ + e^-$ spectrum from 50 GeV to 1 TeV, as originally reported in [7]. To fit the high energy part of the Fermi LAT spectrum and to agree with the H.E.S.S. data, a conventional propagation model requires a power law index $\alpha \simeq 2.5$ above ~ 4 GeV and a cutoff at ~ 2 TeV. However, while providing good agreement with the high energy part of the spectrum, a model with a single power law injection index fails to reproduce the low-energy data.

The spectrum measured with the Fermi LAT suggests some spectral flattening at 70–200 GeV and a noticeable excess above 200 GeV as compared to our power-law spectral fit. These gentle features of the spectrum can be explained within a conventional model by adjusting the injection spectra.
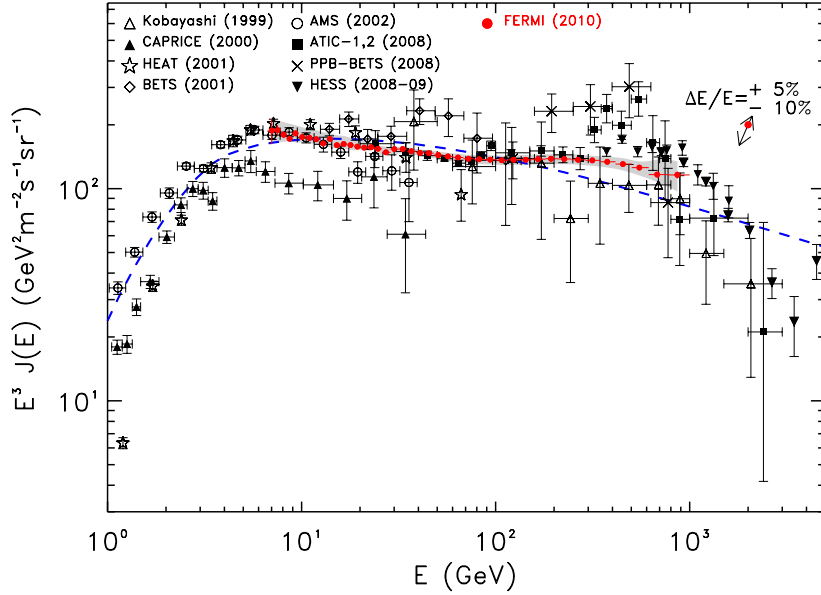
Fig. 5. – Cosmic-ray electron spectrum as measured by Fermi LAT for one year of observations (filled circles, preliminary), with other recent high energy results. Systematic errors are shown by the grey band. The range of the spectrum rigid shift implied by a shift of the absolute energy is shown by the arrow in the upper right corner. Dashed line shows the model based on pre-Fermi results [18]. Data from other experiments are: Kobayashi [19], CAPRICE [20], HEAT [21], BETS [22], AMS [23], ATIC [9], PPB-BETS [10], H.E.S.S. [11, 12]. Note that the AMS data are for e^- only.

Another possibility that provides a good overall agreement with our spectrum is the introduction of an additional leptonic component with a hard spectrum. Such an additional component is motivated by the rise in the positron fraction reported by PAMELA [13]. Recent papers have suggested different models for this component. The data can accommodate a contribution from nearby sources (such as pulsars) or from the annihilation of dark matter particles (see, e.g., [24] for a comprehensive list of references).

The features may also be explained by other astrophysical effects, such as reacceleration of secondary CRs at the source, as in [25] and [26], distribution of the CR acceleration sites, as in [27] and many others.

The different proposed solutions have specific signatures in some CR observables that would help discriminating them. Isolated local sources would give rise to spectral features in the CRE spectrum, secondary CR reacceleration at the source would produce rising fractions of antiprotons over protons and secondary nuclei, e.g., boron over carbon, propagation effects on electrons coming from far-away SNR as in [27] would produce a decrease in the positron fraction at very high energy.

The Fermi Collaboration is actively working on reducing systematic uncertainties on the measurement of the CRE spectrum to be able to identify any possible such feature. Moreover, since an excess of electrons of Dark Matter origin would produce a corresponding excess in the Inverse Compton component of the diffuse gamma-ray emission, our measurement of the extragalactic isotropic diffuse emission [4] already provides powerful constraints on many DM models which are put forward to explain the Fermi and Pamela

lepton excesses [5]. Even more accurate measurements of gamma-ray diffuse emission, that the Fermi Collaboration is actively pursuing, will be crucial to further constrain the manifold DM parameter space. Finally, the Fermi Collaboration has been developing techniques to perform a measurement of small and large scale anisotropies in the arrival direction of electrons [28], in the attempt to detect local sources of electrons, and to perform a measurement of the positron fraction using the Earth magnetic field as a spectrometer to separate leptons of opposite charge.

<p align="center">* * *</p>

REFERENCES

[1] ATWOOD W. B. *et al.*, *Astrophys. J.*, **697** (2009) 1071.
[2] ABDO A. A. *et al.*, *Science*, **325** (2009) 840.
[3] GRANOT J., *Proceedings of The Shocking Universe - Gamma-Ray Bursts and High Energy Shock phenomena*, astro-ph/1003.2452 (2010).
[4] ABDO A. A. *et al.*, *Phys. Rev. Lett.*, **104** (2010) 101101.
[5] ABDO A. A. *et al.*, *J. Cosmol. Astropart. Phys.*, **04** (2010) 014.
[6] ABDO A. A. *et al.*, *Astrophys. J. Suppl. Ser.*, **188** (2010) 405.
[7] ABDO A. A. *et al.*, *Phys. Rev. Lett.*, **102** (2009) 181101.
[8] AHARONIAN F. A., ATOYAN A. M. and VÖLK H. J., *Astron. Astrophys.*, **294** (1995) L41.
[9] CHANG J. *et al.*, *Nature*, **456** (2008) 362.
[10] TORII S. *et al.*, astro-ph/0809.0760 (2008).
[11] AHARONIAN F. *et al.*, *Phys. Rev. Lett.*, **101** (2008) 261104.
[12] AHARONIAN F. *et al.*, *Astron. Astrophys.*, **508** (2009) 561.
[13] ADRIANI O. *et al.*, *Nature*, **458** (2008) 607.
[14] BALL N. M. and BRUNNER R. J., astro-ph/0906.2173 (2009).
[15] SMART D. F. and SHEA M. A., *Adv. Space Res.*, **36** (2005) 2012.
[16] PESCE-ROLLINS M., *Proceedings of 2nd Fermi Symposium*, astro-ph/0912.3611 (2009).
[17] SGRÓ C., BREGEON J. and BALDINI L., *Proceedings of 31st ICRC*, astro-ph/ 0907.0385 (2009).
[18] STRONG A. W., MOSKALENKO I. V. and REIMER O., *Astrophys. J.*, **613** (2004) 962.
[19] KOBAYASHI T. *et al.*, *Proceedings of the 26th ICRC* (2009).
[20] BOEZIO M. *et al.*, *Astrophys. J.*, **532** (2000) 653.
[21] DUVERNOIS M. A. *et al.*, *Astrophys. J.*, **559** (2001) 296.
[22] TORII S. *et al.*, *Astrophys. J.*, **559** (2001) 973.
[23] AGUILAR M. *et al.*, *Phys. Rep.*, **336** (2002) 331.
[24] GRASSO D. *et al.*, *Astropart. Phys.*, **32** (2009) 140.
[25] BLASI P., *Phys. Rev. Lett.*, **103** (2009) 051104.
[26] AHLERS M., MERTSCH P. and SARKAR S., *Phys. Rev. D*, **80** (2009) 123017.
[27] SHAVIV J. N., NAKAR E. and PIRAN T., *Phys. Rev. Lett.*, **103** (2009) 111302.
[28] ACKERMANN M *et al.*, *Phys.Rev. D*, **82** (2010) 092003, astro-ph/1008.5119.